Supporting Information

Merchant et al. 10.1073/pnas.1302725110

SI Materials and Methods

Cell lines used were as follows: breast cancer CAL51 [German Collection of Microorganisms and Cell Culture (DSMZ); ACC-302], CAL85-1 (DSMZ; ACC-440), HCC-1143 [American Tissue Type Collection (ATCC); CRL-2321], HCC1937 (ATCC; CRL-2336), HDQ-P1 (DSMZ; ACC-494); colorectal cancer DLD-1 (ATCC; CCL-221), HCT-8 (ATCC; CCL-244), HCT-15 (ATCC; CCL-225); GBM U-87 MG (ATCC; HTB-14); non–small-cell lung cancer (NSCLC) A549 (ATCC; CCL-185), HOP18, HOP92, NCI-H358 (ATCC; CRL-5807), NCI-H441 (ATCC; HTB-174), NCI-H596 (ATCC; HTB-178), NCI-H838 (ATCC; CRL-5844), NCI-H1568 (ATCC; CRL-5876), NCI-H1666 (ATCC; CRL-5885), NCI-H1838 (ATCC; CRL-5899), NCI-H1975 (ATCC; CRL-5908), RERF-LC-Ad1 [Japanese Collection of Research Bioresources (JCRB); JCRB1020), RERF-LC-MS (JCRB, JCRB0081), SK-Mes-1 (ATCC; HTB-58); pancreatic cancer AsPC-1 (ATCC; CRL-1682), BxPC-3 (ATCC; CRL-1687), Capan-1 (ATCC; HTB-79), CFPAC-1 (ATCC; CRL-1918), HPAC (ATCC; CRL-2119), KP4 (Riken Bioresource Center Cell Bank; RCB1005); and renal cancer Caki-1 (ATCC; HTB-46), Caki-2 (ATCC; HTB-47), TK-10 [National Cancer Institute (NCI) Repository], UO-31 (NCI Repository).

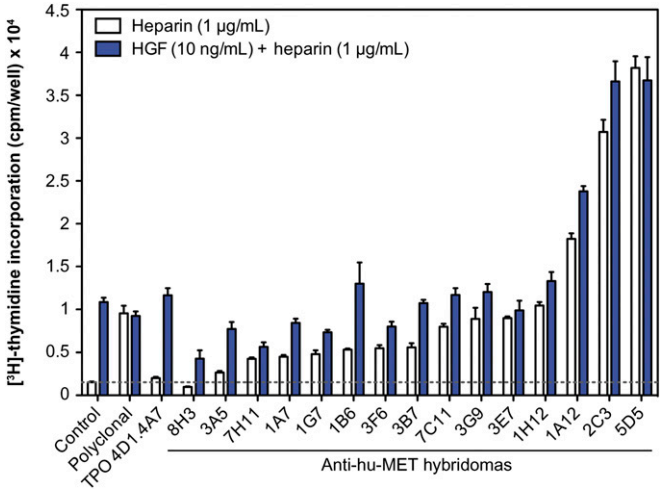

Fig. S1. Effect of anti-receptor tyrosine kinase MET hybridoma antibodies on Ba/F3–human (hu)MET cell proliferation in the presence or absence of HGF. [^{3}H]thymidine-incorporation assays were performed using Ba/F3-huMET cells treated with no treatment (control), anti-MET polyclonal Abs (pAbs), a negative control hybridoma antibody (anti-thrombopoietin antibody; TPO 4D1.4A7), or anti-huMET hybridoma antibodies in the presence (blue bars) or absence (white bars) of hepatocyte growth factor (HGF). HGF and anti-MET pAbs, but not the negative control hybridoma antibody, drive cell proliferation ([^{3}H]thymidine incorporation). The anti-huMET hybridoma antibodies identified in this screen are plotted in order of their ability to agonize cell proliferation. The 5D5 antibody increased cell proliferation roughly 2,500% in the presence or absence of HGF.

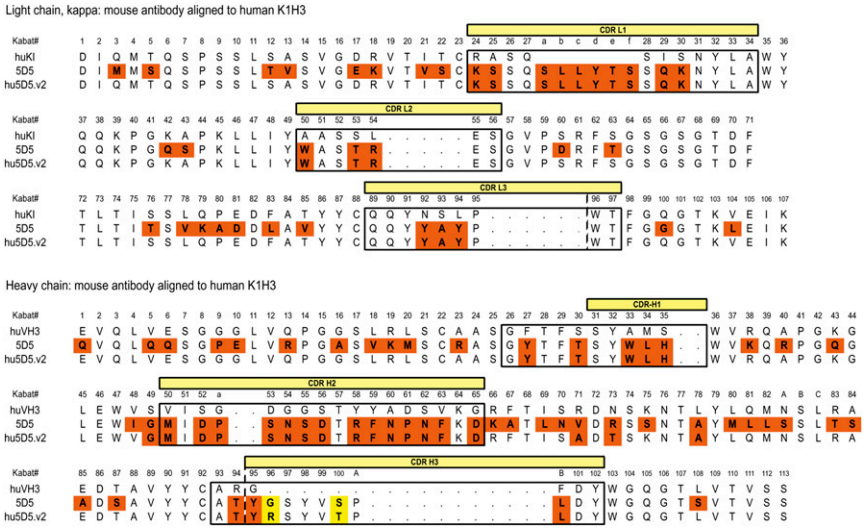

Fig. S2. Sequence alignment of the 5D5 and 5D5 version 2 (5D5.v2) anti-MET antibodies with human consensus frameworks. Variable domain sequences of the 5D5 variants aligned with human consensus κI variable light (VL) and subgroup 3 variable heavy (VH3) domain frameworks. Amino acid positions that differ from the human consensus are highlighted in orange; regions that were transferred to generate the complementarity-determining region (CDR) graft are boxed. Positions are numbered according to Kabat (1).

1. Kabat EA, Wu TT, Perry HM, Gottesman KS, Foeller C (1991) *Sequences of Proteins of Immunological Interest* (Public Health Service, National Institute of Health, Bethesda, MD).

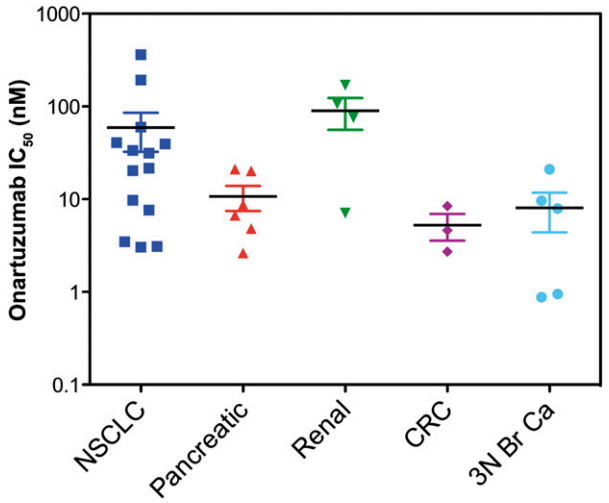

Fig. S3. Inhibition of HGF-dependent cell proliferation by onartuzumab across multiple cancer cell lines by tumor type. IC_{50} values for inhibition of HGF-dependent cell proliferation by onartuzumab across NSCLC, pancreatic, renal, colorectal cancer (CRC), and triple-negative breast cancer (3N Br Ca) cell lines are summarized.

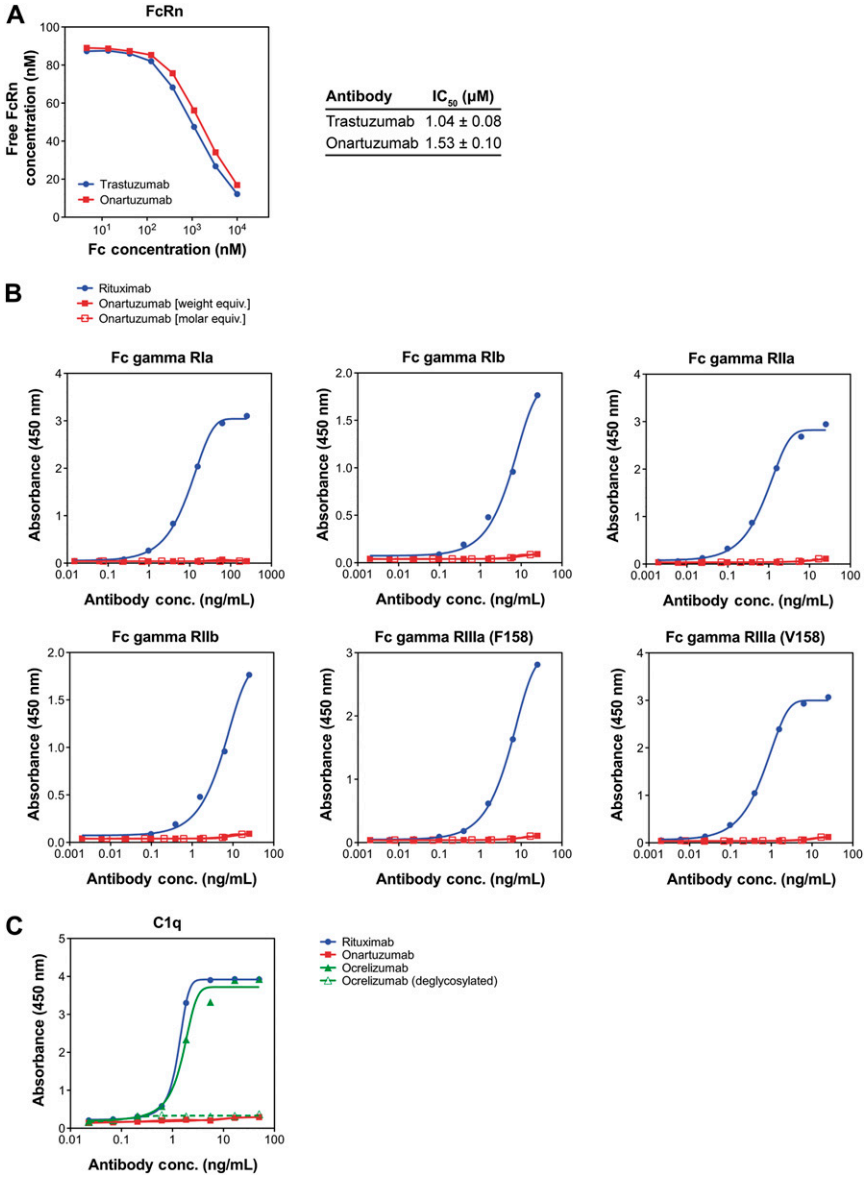

Fig. S4. Evaluation of neonatal constant domain fragment (Fc) receptor (FcRn), Fcγ receptors, and C1q binding to onartuzumab. (*A*) Onartuzumab binds to FcRn with similar affinity as that of trastuzumab with calculated IC_{50} values of 1.53 and 1.04 μM, respectively. (*B*) Onartuzumab shows no binding to FcγRIa, FcγRIIa, FcγRIIb, FcγRIIIa (F158), or FcγRIIIa (V158) when tested at equal weight or molarity to a positive control antibody, rituximab, which shows binding to all Fcγ receptors tested. (*C*) Onartuzumab shows no binding to the complement protein C1q, whereas the positive control antibodies rituximab and ocrelizumab bind C1q as expected. A deglycosylated version of ocrelizumab shows no binding to C1q.

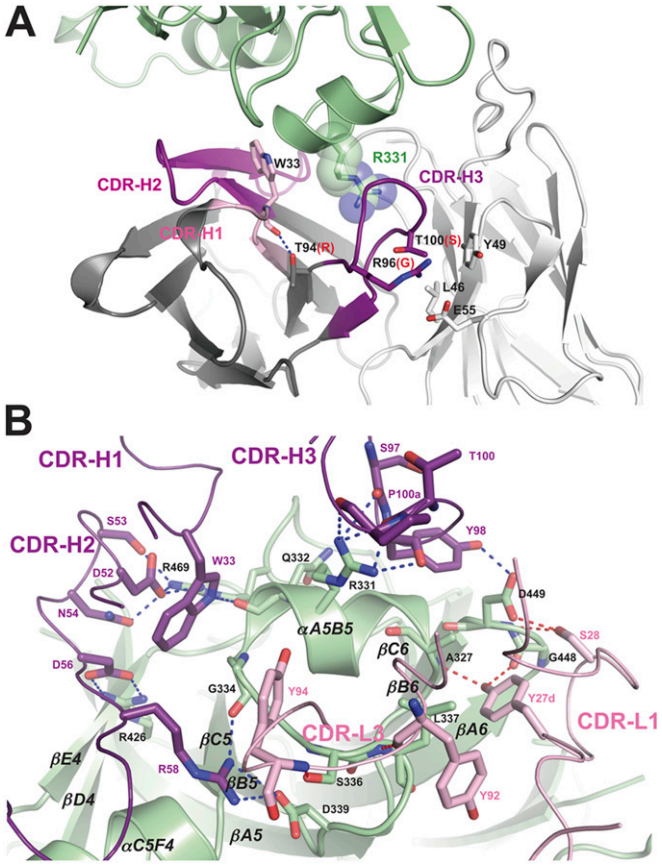

Fig. S5. Structural details of the interaction between the onartuzumab Fab and MET. (*A*) Structural basis of the onartuzumab (5D5.v2) CDR repair and affinity maturation. The MET Sema (light green), humanized onartuzumab heavy chain (dark gray), and light chain (light gray) are depicted. The humanized onartuzumab heavy chain CDR loops 1, 2, and 3 are colored light pink, magenta, and deep purple, respectively. The residues that emerged from CDR repair and affinity maturation and their interaction partners are depicted as sticks. Blue dotted lines indicate hydrogen bonds. The changes made at four positions in the CDR-H3 during affinity maturation led to an overall affinity improvement of 14-fold, largely attributable to a fivefold decrease in the dissociation rate. During humanization, a single change, R94S in the VH domain (onartuzumab), led to an affinity similar to murine 5D5. The obligate R94 to S/T mutation in onartuzumab, required for restoring MET binding, is anchored to the main-chain oxygen atom of CDR-H1 residues W33 via a hydrogen bond. Moreover, the G96R and S100T amino acid changes identified from affinity maturation further bolster hydrophobic or van der Waals contacts between CDR-H3 and CDR-L2. Together, although Thr94, Arg96, and Thr100 are not directly involved in the antigen recognition, they stabilize the overall conformation of CDR-H3, and facilitate the projection of CDR-H3 loop toward the helix αA5B5 in MET. (*B*) Interactions between humanized onartuzumab and MET Sema PSI. Important interfacial side chains are shown as sticks with nitrogen atoms in blue, oxygen atoms in red, and carbon atoms in light green (MET), deep purple (onartuzumab heavy chain), and light pink (onartuzumab light chain). Blue and red dotted lines indicate hydrogen bonds between MET and onartuzumab heavy chain and light chain, respectively.

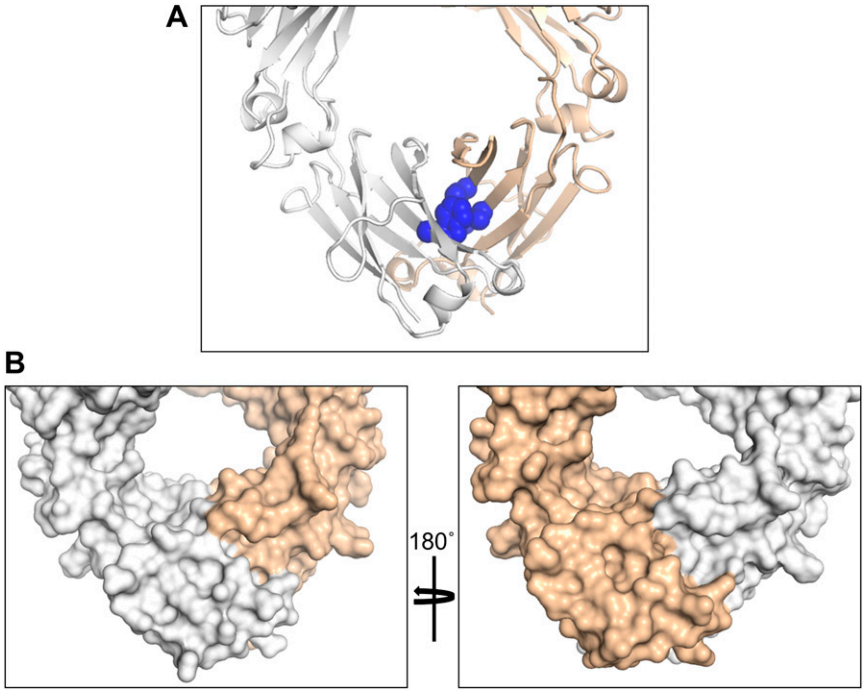

Fig. S6. Structural depiction of the location of the "knob" and "hole" mutations within the C_H3 domain of the Fc in onartuzumab. (*A*) The knob and hole mutations are highlighted in blue within the C_H3 domain of the Fc domain as predicted and shown in a ribbon diagram. (*B*) A space-filling model of the onartuzumab Fc domain depicts the surface exposed residues in the Fc domain, revealing no solvent exposure of the knob and hole residues (in blue).

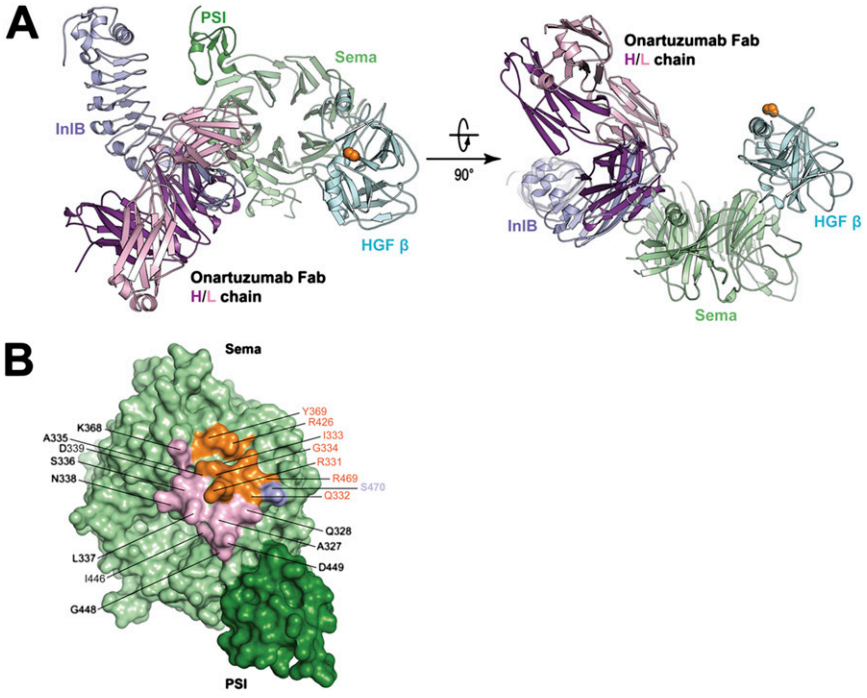

Fig. S7. Onartuzumab binding site on MET overlaps with the secondary binding site of the *Listeria monocytogenes* protein Internalin (Inl)B on MET. (*A*) Two orthogonal views of the overlay of the onartuzumab/MET Sema PSI/HGF-β complex with MET/InlB complex (Protein Data Bank ID code 2UZX) based on the Sema domain (residues 42–515). The InlB from the MET/InlB complex is shown in light blue and the rest of the color scheme is according to Fig. 4*D*. (*B*) Onartuzumab epitope on MET overlaps with the InlB secondary-binding sites. Surface representation of MET Sema PSI shows residues involved in onartuzumab binding (light pink), InlB binding (light blue), or both (orange).

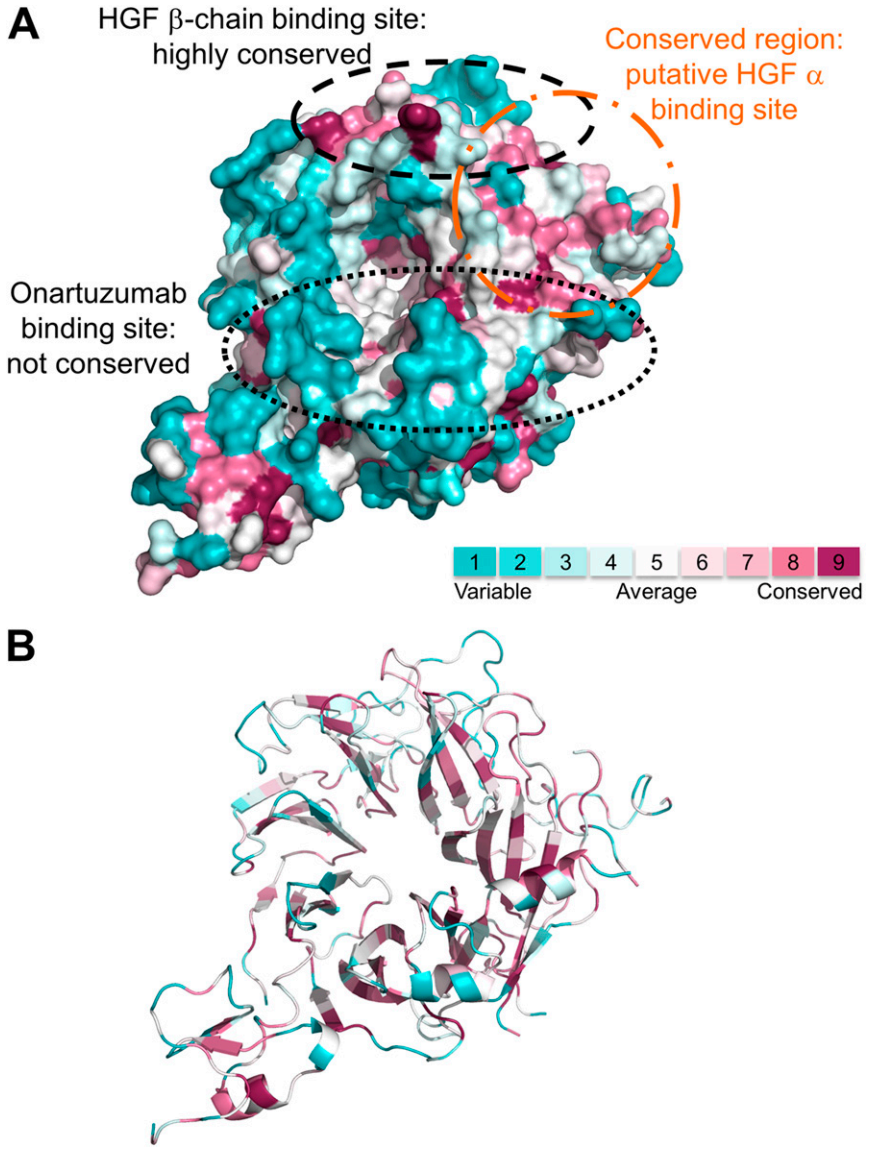

Fig. S8. Structural visualization of the sequence conservation of the MET Sema domain from multiple species. Surface representation of the MET Sema domain residues that are conserved (red) or nonconserved (aqua) between human (*Homo sapiens*) and 10 other species, including *Lemur catta*, *Equus caballus*, *Bos taurus*, *Sus scrofa*, *Mus musculus*, *Rattus norvegicus, Gallus gallus*, *Xenopus laevis*, *Danio rerio*, and *Tetraodon nigroviridis* are depicted as surface-rendered (*A*) and ribbon (*B*) diagrams. The known interaction sites for HGF-β (black dashed oval) and onartuzumab (black dotted oval) are indicated. A highly conserved region adjacent to the HGF β-chain and onartuzumab binding sites is highlighted as a putative HGF-α–binding site (orange broken line circle). The figures were prepared by ConSurf server (http://consurf.tau.ac.il).

Table S1. X-ray data collection, phasing, and refinement statistics for MET Sema-PSI, onartuzumab Fab, and HGF-β ternary complex

Crystal	Native
Space group	$P2_12_12$
Cell dimension	
a, *b*, *c* (Å)	128.2, 192.2, 65.6
α, β, γ (°)	90, 90, 90
Resolution, Å	50.0–2.80 (2.90–2.80)
R_{sym}*	7.4 (51.3)
I/σI	15.6 (1.9)
Completeness, %	98.9 (98.0)
Redundancy	4.0 (3.8)
Refinement	
Resolution, Å	50.0–2.80 (2.90–2.80)
No. of reflections	38,286
R_{work}/R_{free}, %	21.1/25.3
No. of atoms	
Protein	9,084
Ligand/ion	14
Water	183
B-factors†, Å^2	
Protein	50
Ligand/ion	48
Water	43
r.m.s. deviations	
Bond lengths, Å	0.007
Bond angles, °	1.05

X-ray diffraction data were collected from a single crystal. Values in parentheses represent the highest resolution shell.

*$R_{sym}(I) = \Sigma hkl \Sigma i \left| Ii(hkl) - \langle I(hkl) \rangle \right| / \Sigma hkl \Sigma i Ii(hkl)$ where the summations are over i observations of each reflection and all hkl. ⟨I(hkl)⟩ is the average intensity of the i observations. $Rwork = \left| F(obs) - F(calc) \right| / F(obs)$.

†R_{free} is calculated for 5% of randomly selected reflections not used in the refinement.